ChemPubSoc Europe

DOI: 10.1002/chem.201304962

CHEMISTRY
A European Journal
Full Paper

Metal–Organic Frameworks

The Adsorption and Simulated Separation of Light Hydrocarbons in Isoreticular Metal–Organic Frameworks Based on Dendritic Ligands with Different Aliphatic Side Chains

Jiangtao Jia,[a] Lei Wang,[a] Fuxing Sun,[a] Xiaofei Jing,[a] Zheng Bian,*[b] Lianxun Gao,[b] Rajamani Krishna,[d] and Guangshan Zhu*[a, c]

Abstract: Three isoreticular metal–organic frameworks, JUC-100, JUC-103 and JUC-106, were synthesized by connecting six-node dendritic ligands to a $[Zn_4O(CO_2)_6]$ cluster. JUC-103 and JUC-106 have additional methyl and ethyl groups, respectively, in the pores with respect to JUC-100. The uptake measurements of the three MOFs for CH_4, C_2H_4, C_2H_6 and C_3H_8 were carried out. At 298 K, 1 atm, JUC-103 has relatively high CH_4 uptake, but JUC-100 is the best at 273 K, 1 atm. JUC-100 and JUC-103 have similar C_2H_4 absorption ability. In addition, JUC-100 has the best absorption capacity for C_2H_6 and C_3H_8. These results suggest that high surface area and appropriate pore size are important factors for gas uptake. Furthermore, ideal adsorbed solution theory (IAST) analyses show that all three MOFs have good C_3H_8/CH_4 and C_2H_6/CH_4 selectivities for an equimolar quaternary $CH_4/C_2H_4/C_2H_6/C_3H_8$ gas mixture maintained at isothermal conditions at 298 K, and JUC-106 has the best C_2H_6/CH_4 selectivity. The breakthrough simulations indicate that all three MOFs have good capability for separating C2 hydrocarbons from C3 hydrocarbons. The pulse chromatographic simulations also indicate that all three MOFs are able to separate $CH_4/C_2H_4/C_2H_6/C_3H_8$ mixture into three different fractions of C1, C2 and C3 hydrocarbons.

Introduction

The chemical and petroleum industry can produce a large amount mixed light-hydrocarbon gases containing CH_4, C_2H_4, C_2H_6, C_3H_8, and so forth. These gases are important sources for the advanced chemicals in industry. For example, CH_4 can be used to prepare acetylene or formalin and C_2H_4 is a starting material for synthetic fiber or plastics. In general, high purity hydrocarbon gas is a prerequisite for these chemical transformation procedures. In order to fully utilise light-hydrocarbon resources, it is essential and important to explore the methods to efficiently separate the mixed light hydrocarbons into pure components. Notably, the traditional separation method, such as cryogenic distillation, consumes more energy. Recent advances have shown that adsorptive separation using the porous materials could provide an opportunity for low-energy consumption.[1]

Porous metal–organic frameworks (MOFs) have attracted much attention in the last decade, because they have various potential applications, such as gas uptake,[2] separation,[1c,3] sensing,[4] catalysis,[5] light harvesting,[6] and so on. Recently, MOFs have been considered as separation materials for light hydrocarbons owing to diverse metal sites and tunable pores. Long et al. have studied the effects of different metal sites for C_2H_4 and C_2H_6 separation.[7] Chen et al. have also investigated many different MOFs for the ability for C1, C2 and C3 light hydrocarbons.[1c] However, the factors that affect the separation of C1, C2 and C3 light hydrocarbons are not very clear. It may be a valuable trial to solve the problem by isoreticular MOFs with different substituted groups.

In recent years, our research efforts have focused on the design of MOFs by connecting dendritic organic building blocks and inorganic building blocks. A six-node dendritic ligand 1,3,5-tris[3,5-di(4-carboxyphenyl-1-yl)phenyl-1-yl]benzene (**L1**), which does not contain any aliphatic groups (Figure 1 a) and can be seen as an octahedral organic building block (Figure 1 b), can combine with the trigonal prismatic $[In_3O(CO_2)_6]$ cluster (Figure 1 d) to form a MOF with **nia** topology (JUC-101, Figure 1 g).[8] It can also be used to construct

[a] *Dr. J. Jia, L. Wang, F. Sun, X. Jing, Prof. G. Zhu*
State Key Laboratory of Inorganic Synthesis and Preparative Chemistry
College of Chemistry, Jilin University, Changchun (China)
E-mail: zhugs@jlu.edu.cn

[b] *Dr. Z. Bian, Prof. L. Gao*
State Key Laboratory of Polymer Physics and Chemistry
Changchun Institute of Applied Chemistry
Chinese Academy of Sciences, Changchun (China)
E-mail: bianzh@ciac.ac.cn

[c] *Prof. G. Zhu*
Griffith School of Environment
Griffith University, Queensland (Australia)

[d] *Prof. R. Krishna*
Van 't Hoff Institute for Molecular Sciences
University of Amsterdam
Science Park 904,1098 XH Amsterdam (The Netherlands)

Supporting information for this article is available on the WWW under http://dx.doi.org/10.1002/chem.201304962.

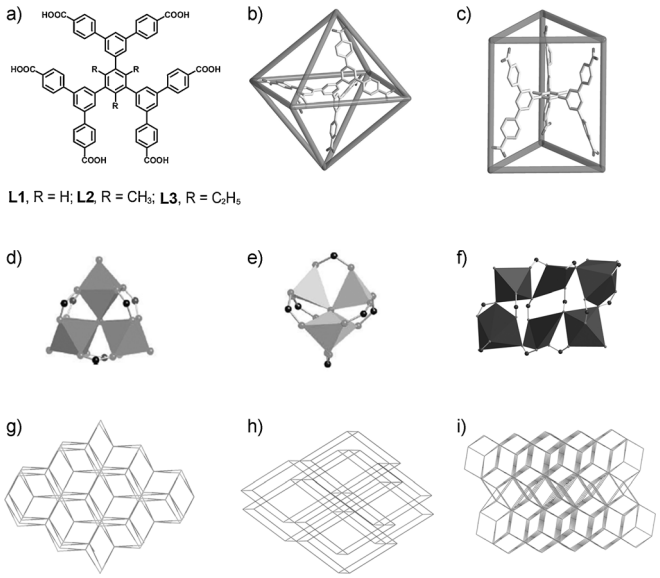

Figure 1. Constructing MOFs by reticular chemistry. a) Ligand **L1**, **L2** and **L3**; b) octahedral organic building block; c) trigonal prismatic organic building block; d) $[In_3O(CO_2)_6]$ cluster; e) $[Zn_4O(CO_2)_6]$ cluster; f) $[Pb_6(CO_2)_{12}]$ cluster; g) **nia** topology; h) two interpenetrated network **pcu** topology; i) $CaSi_2$ topology.

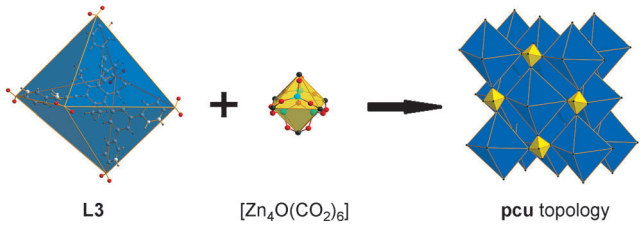

Figure 2. Constructing JUC-106 from **L3** and $[Zn_4O(CO_2)_6]$ cluster.

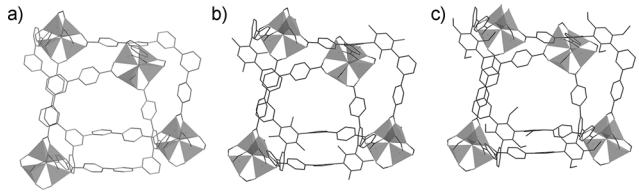

Figure 3. The cages of a) JUC-100, b) JUC-103 and c) JUC-106.

a two interpenetrating MOF network with **pcu** topology (JUC-100, Figure 1 h) by utilising the octahedral $[Zn_4O(CO_2)_6]$ cluster (Figure 1 e).[9] Another six-node dendritic ligand 2,4,6-trimethyl-1,3,5-tri[3,5-di(4-carboxyphenyl-1-yl)phenyl-1-yl]benzene (**L2**; Figure 1 a) with a trigonal prismatic conformation (Figure 1 c) was used to form a (6,12)-connected $CaSi_2$ topology (JUC-105, Figure 1 i) with the 12-connected $[Pb_6(CO_2)_{12}]$ cluster (Figure 1 f). Very interestingly, when **L2** was combined with the octahedral $[Zn_4O(CO_2)_6]$, cluster, a two interpenetrating MOF network (JUC-103) with **pcu** topology was obtained, and the conformation of **L2** was twisted to octahedron.[10] JUC-103 and JUC-100 have the isoreticular structure.

In this paper, we further synthesize the similar ligand 1,3,5-triethyl-2,4,6-[3,5-di(4-carboxyphenyl-1-yl)phenyl-1-yl]benzene (**L3**; Figure 1 a), which also can combine with octahedral $[Zn_4O(CO_2)_6]$ cluster to form a two-interpenetrating MOF network (JUC-106) with **pcu** topology. The effects of three isoreticular MOF materials with different side chains, JUC-100, JUC-103 and JUC-106, for the uptake and separation of light hydrocarbon are systematically studied.

Results and Discussion

Structures

The assembly strategy of JUC-106 is almost identical to those of JUC-100 and JUC-103 reported previously (Figures 2 and 3). Single-crystal diffraction analysis reveals that JUC-106 crystallizes in the trigonal space group $R\bar{3}c$. The asymmetric unit (see Supporting Information) of JUC-106 contains two zinc(II) ions, one third of the **L3** ligand, and one bridging μ_4-O atom. The zinc(II) ions are four-coordinated with three oxygen atoms from the carboxylates and the bridging μ_4-O atom. Four zinc(II) ions, six carboxyl groups and one bridging μ_4-O atom form a $[Zn_4O(CO_2)_6]$ cluster. The $[Zn_4O(CO_2)_6]$ cluster is linked by six 6-connected dendritic ligands to give two interpenetrating networks. The $[Zn_4O(CO_2)_6]$ cluster and the 6-connected dendritic ligand can both be simplified to 6-connected nodes with octahedral configuration. By using the TOPOS program, JUC-106 was found to display a **pcu** topology with the Schläfli symbol $(4^{12}\cdot6^3)$. The powder XRD pattern of the as-made JUC-106 coincides with the simulated one (see Supporting Information).

It should be noted that JUC-100 and JUC-103 have the same symmetry and similar network to JUC-106, and their structures can be transformed each other by the replacement of ligands. There are still some differences in the unit cell dimensions. With the methyl and ethyl unit on the central phenyl ring of the ligand, the *a* and *b* axes of JUC-103 and JUC-106 become shorter and the *c* axis becomes longer compared to JUC-100 (see Supporting Information). Evidently, these aliphatic units can cause a larger twist of adjacent phenyl rings. Notably, the computational results showed that the most stable configuration of **L3** also is a trigonal prism. In addition, the substituent units affect the distance of the two interpenetrated structures. The distances between central phenyl ring of one ligand and the μ_4-O atom of the adjacent metal cluster belonging to the other interpenetrated structure are 5.609, 6.418 and 6.457 Å in JUC-100, JUC-103 and JUC-106, respectively. The distance increases with the increasing volume of the substituent units. Observed from the inside of the cage, it can be found that the methyl and ethyl substituents cover the phenyl rings in the other interpenetrated structure (Figure 4).

Four $[Zn_4O(CO_2)_6]$ clusters and four ligands form an irregular cubic cage, and two cages interpenetrate each other to form a bigger one in which one $[Zn_4O(CO_2)_6]$ cluster is adjacent to the central phenyl ring from the other interpenetrated structure (Figure 3). Therefore, six ethyl units are directed to the interior of the cage, similar to JUC-103. The distance between

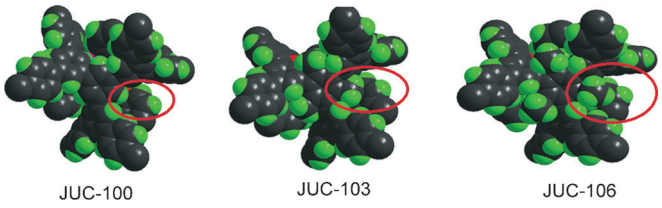

Figure 4. The cages observed from the inside. The substituents are marked in the circles.

two interpenetrated structures and the volume of the substituents affect the pore size of the MOFs. The pore sizes for JUC-100, JUC-103 and JUC-106 are calculated to be about 14, 10 and 8 Å, respectively. The calculated framework densities of desolvated JUC-100, JUC-103 and JUC-106 are 0.888, 0.933 and 0.963 g cm^{-3}, respectively. The thermo-gravimetric (TG) curve of JUC-106 displays a platform without weight loss from 200 to 400 °C. The PXRD pattern of JUC-106 after the sample heated at 350 °C for 2 h is almost identical to the obtained single-crystal data, indicating high thermal stability of JUC-106 (see Supporting Information).

N_2 Adsorption

The N_2 uptakes of JUC-100, JUC-103 and JUC-106 at 77 K, 1 atm are 652, 384 and 305 cm^{3}g^{-1} (Figure 5), respectively. All of the adsorption curves are type-I isotherms. The isotherm of JUC-100 appears to have hysteretic sorption behaviour because of dynamic features and the cage effect.[9,11] However, this hysteretic sorption behaviour is not found in JUC-103 and JUC-106, possibly owing to the fact that the reduction of pore dimensions weakens the cage effect. Fitting to the N_2 isotherm curve, the BET surface areas of JUC-100, JUC-103 and JUC-106 are 2040, 1484 and 1122 m^{2}g^{-1}, respectively. It can be seen that the BET surface area decreases with the increase of the volume of substituent.

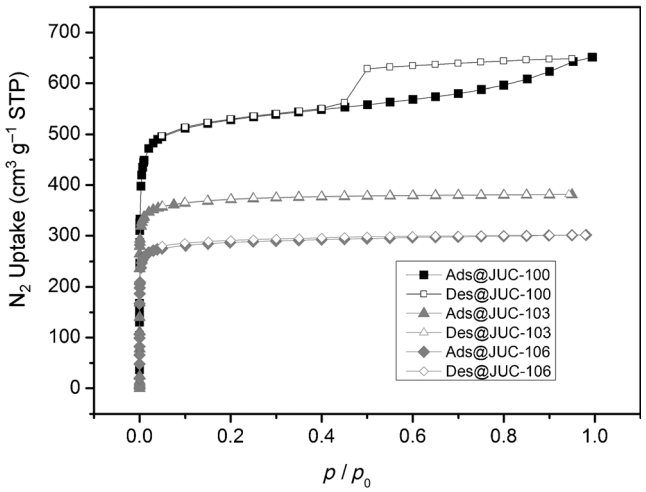

Figure 5. N_2 uptake of JUC-100, JUC-103 and JUC-106.

CH_4 Adsorption

The CH_4 adsorption isotherms of JUC-100, JUC-103 and JUC-106 were tested at 273 K and 298 K, 1 atm. The kinetic diameter of CH_4 molecule with nondipolar, nonquadrupolar, and isotropic shape is 3.8 Å. The uptakes of JUC-100, JUC-103 and JUC-106 are 21.2, 20.1, 16.7 cm^{3}g^{-1} at 273 K, and 10.2, 11.7, 8.14 cm^{3}g^{-1} at 298 K, respectively (Figure 6). The uptakes of CH_4 at 273 K show that the MOF with higher surface area has larger CH_4 uptake. Very interestingly, the CH_4 uptake of JUC-103 at 298 K is larger than those of the others. This suggests that appropriate pore size and temperature are factors that affect CH_4 adsorption.[12]

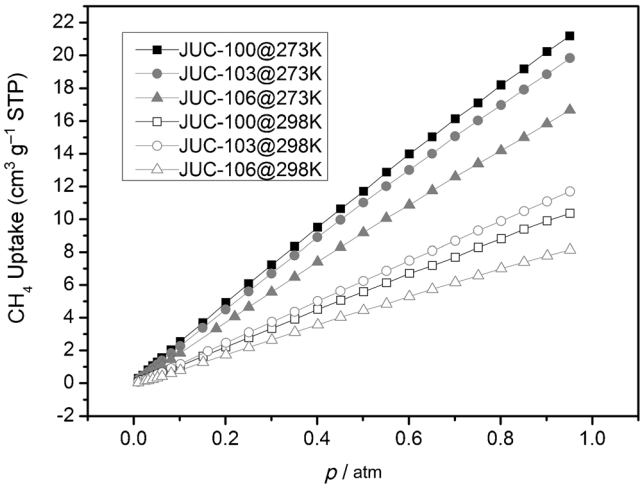

Figure 6. CH_4 uptake of JUC-100, JUC-103 and JUC-106 at 1 atm.

C_2H_6 Adsorption

The kinetic diameter of C_2H_6 is 4.4 Å, which is larger than that of CH_4. The C_2H_6 adsorption isotherms were also tested. The C_2H_6 uptakes of JUC-100, JUC-103 and JUC-106 are 147, 127, and 118 cm^{3}g^{-1} at 273 K and 1 atm, respectively, and 92.1, 85.6 and 78.2 cm^{3}g^{-1}, respectively, at 298 K and 1 atm (Figure 7).

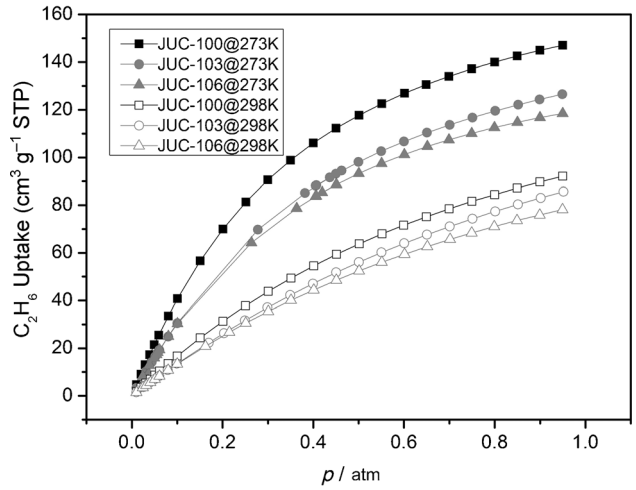

Figure 7. C_2H_6 uptake of JUC-100, JUC-103 and JUC-106 at 1 atm.

For C_2H_6 adsorption, the MOF with the highest surface area has the largest uptake capability. From the adsorption data, it is found that the addition of methyl and ethyl units in the pores reduces the uptake of C_2H_6.

C_2H_4 and C_3H_8 Adsorption

The C_2H_4 and C_3H_8 adsorption of JUC-100, JUC-103 and JUC-106 were also tested at 298 K, 1 atm (Figures 8 and 9). The values of C_2H_4 uptake of JUC-100, JUC-103 and JUC-106 are 114, 111 and 89.6 cm^3g^{-1} at 273 K, 1atm, respectively, and are 66.3, 66.9, and 50.0 cm^3g^{-1} at 298 K, 1 atm, respectively. The C_2H_4 absorption curves of JUC-100 and JUC-103 are almost identical. The values of C_3H_8 uptake of JUC-100, JUC-103 and JUC-106 are 155, 138 and 121 cm^3g^{-1}, respectively, at 273 K, 1 atm, and are 136, 122 and 114 cm^3g^{-1} at 298 K, 1 atm, respectively. JUC-100 displays the best C_3H_8 uptake capacity.

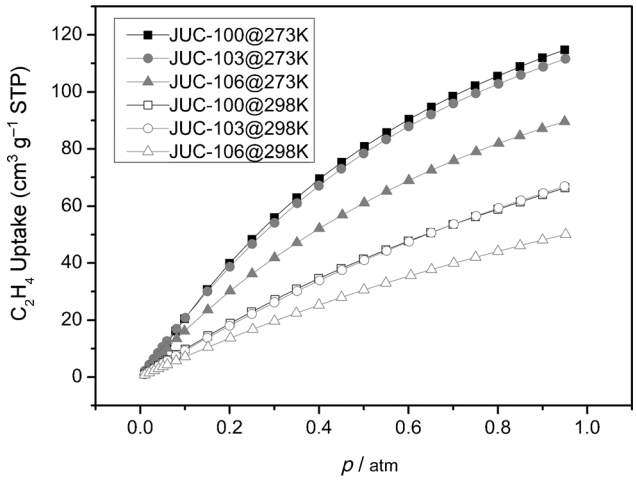

Figure 8. C_2H_4 uptake of JUC-100, JUC-103 and JUC-106 at 1 atm.

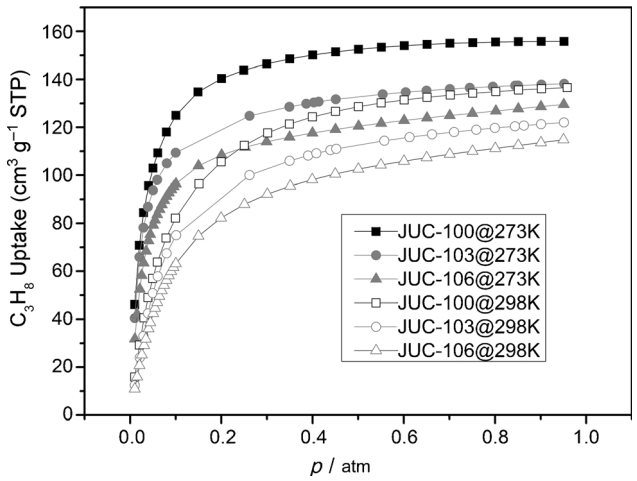

Figure 9. C_3H_8 uptake of JUC-100, JUC-103 and JUC-106 at 1 atm.

The heats of absorption for CH_4, C_2H_6 and C_2H_4

The heats of adsorption for these light carbons of JUC-100, JUC-103 and JUC-106 have been calculated (see Supporting Information). The CH_4 initial adsorption heats of JUC-100, JUC-103 and JUC-106 are −27.1, −23.5 and −26.1 kJ mol^{-1}, respectively. The C_2H_6 initial adsorption heats of JUC-100, JUC-103 and JUC-106 are −26.1, −22.6 and −24.2 kJ mol^{-1}, respectively. The C_2H_4 initial adsorption heats of JUC-100, JUC-103 and JUC-106 are −23.7, −22.8 and −24.2 kJ mol^{-1}, respectively. These data suggest that methyl or ethyl side chains affect little to the absorption heat of gas.

Adsorption selectivity and transient breakthroughs

Figure 10 presents the ideal adsorbed solution theory (IAST) calculations of C_3H_8/CH_4, C_2H_6/CH_4, and C_2H_6/C_2H_4 selectivities for equimolar quaternary $CH_4/C_2H_4/C_2H_6/C_3H_8$ gas mixture maintained at isothermal conditions at 298 K.[13] The C_3H_8/CH_4 selectivity is the highest and falls in the range of 65–150 for JUC-100, JUC-103, and JUC-106. The C_2H_6/CH_4 selectivity is lower and the values are in the range of 8–16 for the three adsorbents. The C_2H_6/C_2H_4 selectivity is the lowest and the values fall in the range of 1.4–2. The low C_2H_6/C_2H_4 selectivity value suggests that sharp separation of C_2H_6 and C_2H_4 is not possible, which will be demonstrated by breakthrough simulations below. In contrast, JUC-106 displays the best separation selectivity for C_2H_6/CH_4 among the three MOFs. JUC-106 and JUC-100 have the similar separation ability for C_3H_8/CH_4.

The methodology used for the breakthrough simulations is the same as that described in earlier work.[14] Experimental validation of the breakthrough simulation methodology is available in the published literature.[14a,15] Figure 11 shows the breakthrough simulations for the three MOFs. The sequence of breakthroughs is CH_4, C_2H_4, C_2H_6, and C_3H_8. The x axis in Figure 11 is dimensionless time τ, defined by dividing the actual time (t) by the characteristic time ($L\varepsilon/u$). The breakthrough hierarchy is dictated by the adsorption strengths; the weaker the adsorption, the earlier the breakthrough. There is a significant time interval between the breakthrough of C_2H_6 and C_3H_8; this indicates that all three MOFs have good capability for separating C2 hydrocarbons from C3 hydrocarbons. The breakthrough times of C_3H_8 for JUC-100, JUC-103, and JUC-106 are $\tau = 540$, 500 and 460, respectively. This decreasing breakthrough time of C_3H_8 is due to progressively lower uptake capacities, as mentioned above. The MOF with the highest pore volume, JUC-100, has the longest breakthrough time. Longer breakthrough times are desirable. because the frequency at which the bed needs to be regenerated is lower, which leads to higher productivity.

The breakthrough simulations in Figure 11 suggest the possibility of separating a mixture of C1, C2 and C3 hydrocarbons into different fractions. To gain further evidence for the fractionation ability of the three MOFs, we performed pulse chromatographic simulations. At the inlet to the adsorber a pulse of a quaternary mixture quaternary $CH_4/C_2H_4/C_2H_6/C_3H_8$ gas mixture is injected for a duration of 10 s. The simulated results are

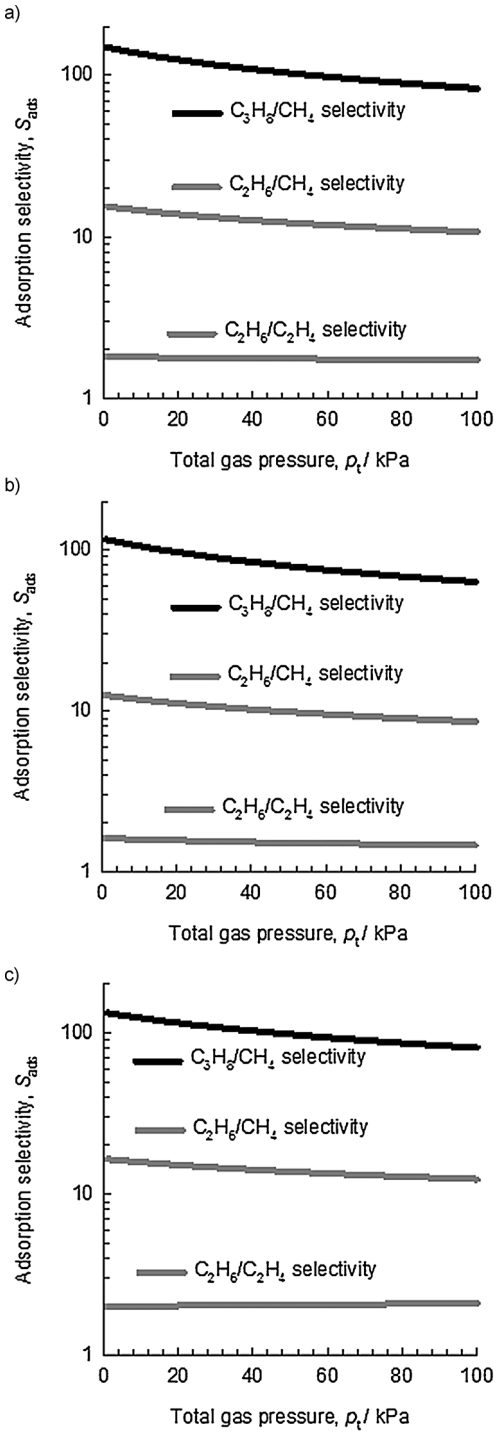

Figure 10. Calculations using ideal adsorbed solution theory (IAST) of Myers and Prausnitz[16] for C_3H_8/CH_4, C_2H_6/CH_4, and C_2H_6/C_2H_4 selectivities for equimolar quaternary $CH_4/C_2H_4/C_2H_6/C_3H_8$ gas mixture maintained at isothermal conditions at 298 K using a) JUC-100, b) JUC-103, and c) JUC-106.

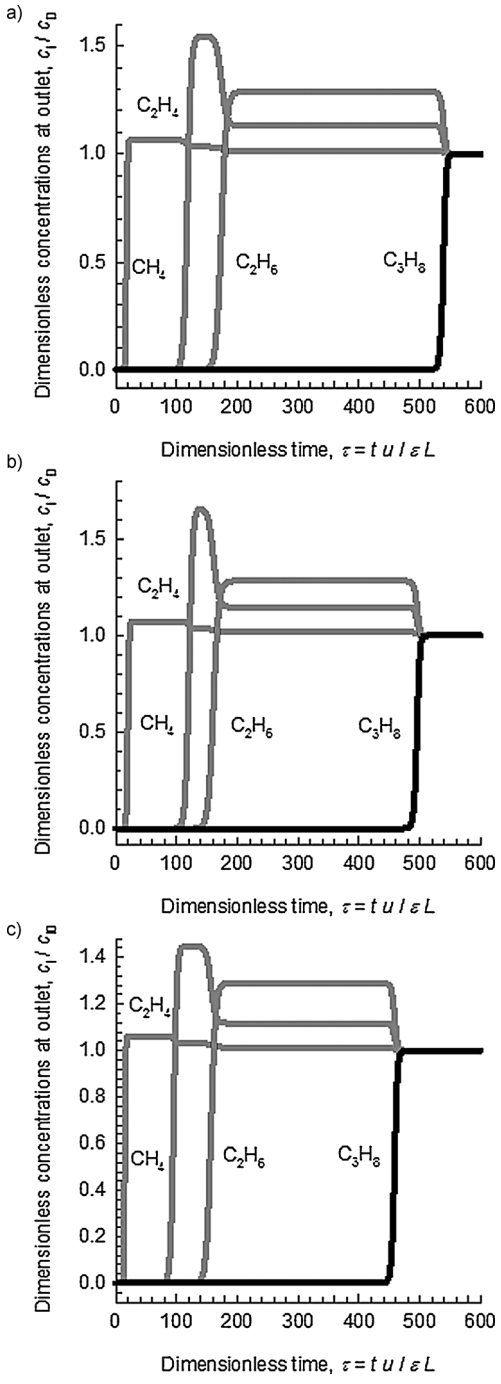

Figure 11. Breakthrough characteristics of the adsorber packed in a) JUC-100, b) JUC-103, and c) JUC-106 and maintained at isothermal conditions at 298 K. The inlet gas is a quaternary $CH_4/C_2H_4/C_2H_6/C_3H_8$ gas mixture maintained at isothermal conditions at 298 K and 100 kPa, with partial pressures for each component of 25 kPa.

shown in Figure 12. For all three MOFs, we are able to separate the mixture of hydrocarbons into three different fractions. The separation between C_2H_4 and C_2H_6 is not sharp, which is due to the relatively low value of the C_2H_6/C_2H_4 adsorption selectivity, as shown in Figure 10.

Conclusion

In conclusion, three isoreticular metal–organic frameworks were synthesized with dendritic ligands that have different aliphatic side chains. The adsorption of the three MOFs for CH_4, C_2H_4, C_2H_6 and C_3H_8 were tested. High surface area and appropriate pore size play key roles for gas adsorption. Furthermore,

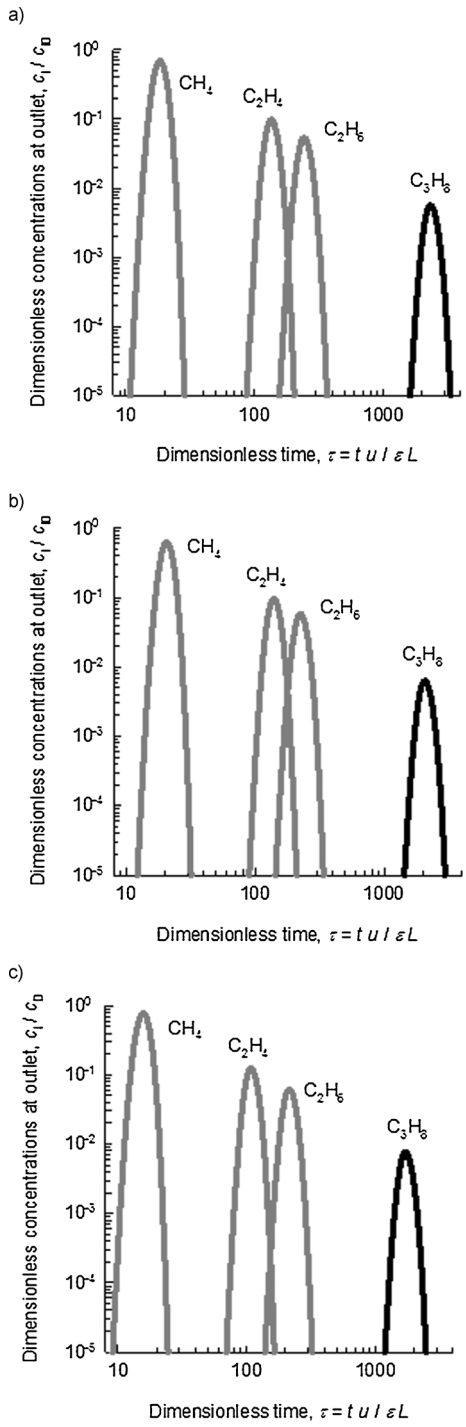

Figure 12. Pulse chromatographic simulations of the adsorber packed in a) JUC-100, b) JUC-103, and c) JUC-106 and maintained at isothermal conditions at 298 K. At the inlet to the adsorber a pulse of a quaternary $CH_4/C_2H_4/C_2H_6/C_3H_8$ gas mixture was injected for a duration of 10 s.

IAST analyses show that all three MOFs have good C_3H_8/CH_4 and C_2H_6/CH_4 selectivities, and JUC-106 has the best C_2H_6/CH_4 selectivity. The breakthrough simulations and pulse chromatographic simulations display that all three MOFs are able to separate $CH_4/C_2H_4/C_2H_6/C_3H_8$ mixture into three different fractions effectively (C1, C2 and C3 hydrocarbons).

Experimental Section

General method

All the chemical reagents used were purchased from commercial sources, unless otherwise noted. Powder X-ray diffractions (PXRD) were collected on a Scintag X1 diffractometer with $Cu_{K\alpha}$ ($\lambda =$ 1.5418 Å) at 50 kV, 200 mA. Thermogravimetric analysis (TGA) measurements were performed at a PerkinElmer TGA 7 thermogravimetric analyser with a heating rate of 10 °C min^{-1} in air. ^{1}H NMR spectra were collected using a VARIAN 300 spectrometer at 298 K. Tetramethylsilane (TMS) of internal standard in ^{1}H NMR experiments was used. Gas adsorption tests were performed with equipment of Autosorb-iQ2-MP-AG.

Synthesis of L3 (see Scheme 1)

Dimethyl 5′-bromo-(1,1′:3′,1″-terphenyl)-4,4″-dicarboxylate (1): 1,3,5-Tribrombenzene (5.0 g, 16 mmol), *p*-methoxylcarbonyl phenylboronic acid (7.2 g, 40 mmol), Na_2CO_3 (8.4 g, 79 mmol), $[Pd(PPh_3)_4]$ (1.3 g, 1.1 mmol) were added to a three-necked flask that contained degassed toluene–methanol–water (80:40:40 mL).

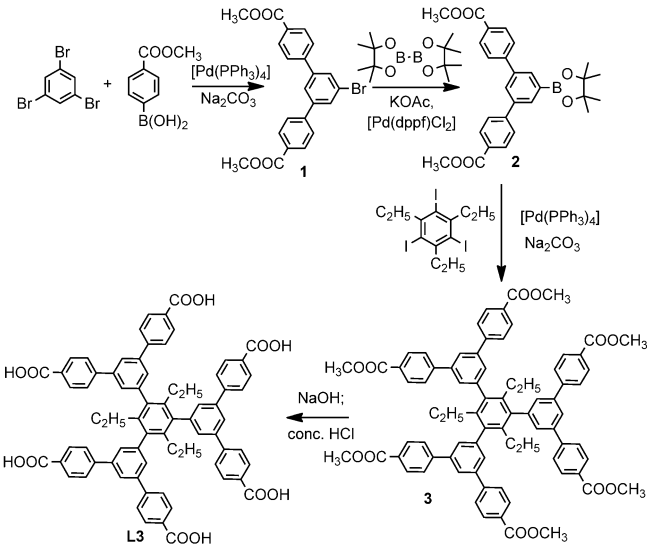

Scheme 1. The synthetic route for the preparation of **L3**.

The solution was stirred under nitrogen atmosphere for 50 h under reflux. The product was extracted using dichloromethane (80 mL × 3), washed with brine (80 mL), and dried with anhydrous $MgSO_4$. The filtered solution was evaporated under reduced pressure. The residue was purified using column chromatography of silica gel (dichloromethane/petroleum ether = 1:2, v/v) to obtain compound **1** (yield: 2.5 g, 37%). ^{1}H NMR (300 Hz, $CDCl_3$): $\delta = 8.15$ (d, $J = 8.0$ Hz, 4H), 7.78 (s, 2H), 7.75 (s, 1H), 7.69 (d, $J = 8.0$ Hz, 4H), 3.96 ppm (s, 6H).

Dimethyl 5′-pinacolatoborontel-(1,1′:3′,1″-terphenyl)-4,4″-dicarboxylate (2): Compound **1** (2.3 g, 5.3 mmol), bis(pinacolato)diboron (1.5 g, 5.7 mmol), KOAc (4.0 g, 40 mmol), and $[Pd(dppf)Cl_2]$ (0.12 g, 0.16 mmol; dppf = 1,1′-bis(diphenylphosphino)ferrocene) were added to a three-necked flask that contained degassed 1,2-dimethoxyethane (100 mL). The solution was stirred for 3 h under reflux to get the product, which was evaporated under reduced pressure. The residue was extracted using dichloromethane

(80 mL×3), washed with brine (80 mL) and dried with anhydrous $MgSO_4$. The filtered solution was evaporated under reduced pressure. The residue was purified using column chromatography of silica gel (dichloromethane/petroleum ether = 1:1, v/v) to obtain **2** (yield: 2.0 g, 78%). ^{1}HNMR (300 Hz, $CDCl_3$): δ = 8.13 (d, J = 8.2 Hz, 4H), 8.09 (d, J = 6.0 Hz, 2H), 7.94 (t, J = 2.0 Hz, 1H), 7.76 (d, J = 8.2 Hz, 4H), 3.95 (s, 6H), 1.39 ppm (s,12H)

1,3,5-Triethyl-2,4,6-tri[3,5-di(4-methoxylcarboxyphenyl-1-yl)-phenyl-1-yl]benzene (3): Compound **2** (0.54 g, 1.0 mmol), Na_2CO_3 (0.53 g, 5.0 mmol) and $[Pd(PPh_3)_4]$ (0.090 g, 0.076 mmol) were added to a three-necked flask that contained degassed toluene (30 mL), ethanol (15 mL) and water (15 mL). The solution was stirred under nitrogen atmosphere for 30 h at 110 °C, and subsequently extracted using dichloromethane (80 mL×3), washed with brine (80 mL), and dried with anhydrous $MgSO_4$. The filtrate was evaporated under reduced pressure. The residue was purified using column chromatography with silica gel (dichloromethane/petroleum ether = 8:1, v/v) to obtain **3** (yield: 0.41 g, 34%). ^{1}H NMR (300 MHz, $CDCl_3$): δ = 8.15 (d, J = 8.4 Hz, 12H), 7.87 (t, J = 1.5 Hz, 3H), 7.77 (d, J = 8.4 Hz, 12H), 7.66 (d, J = 1.5 Hz, 6H), 3.95 (s, 18H), 2.29 (m, 6H), 0.86 ppm (t, J = 7.5 Hz, 9H).

1,3,5-Triethyl-2,4,6-[3,5-di(4-carboxyphenyl-1-yl)phenyl-1-yl]benzene (L3): Compound **3** (0.41 g, 0.34 mmol) and NaOH (2.0 g, 50 mmol) were added to a flask with THF (40 mL), ethanol (40 mL) and water (40 mL). The solution was stirred for 24 h under reflux. At room temperature, the pH value of the solution is adjusted to about 1.0 by concentrated HCl. The resultant white precipitate was filtered to obtain **L3** of 0.33 g (yield: 87%). ^{1}H NMR (300 MHz, $[D_6]$DMSO): δ = 13.02 (s, 6H), 7.98–8.11 (m, 30H), 7.76 (s, 3H,), 2.28 (m, 6H), 0.80 ppm (t, 9H, J = 7.5 Hz).

JUC-106, ((Zn_4O)·(H_2O)·(L3)·(*x* guests)): Compound **L3** (10 mg, 0.0090 mmol) and $Zn(NO_3)_2$·$6H_2O$ (20 mg, 0.067 mmol) were added to a mixed solvent of DMF (3.0 mL) and H_2O (0.60 mL), and then concentrated HNO_3 (0.050 mL) was added. After ultrasonic diffusion, the solution was heated at 85 °C for 72 h to obtain the product of 54% yield (based on ligand) as colourless crystal. Because the guest molecules cannot be resolved in the crystal structure, the exact molecular formula of the MOF with guest molecules cannot be calculated and we could not characterise the element components in the MOFs. Elemental analysis found (%) for JUC-106: C 57.9, H 5.2, N, 5.8. IR: $\tilde{\nu}$ = 3431, 2926, 1675, 1607, 1542, 1403, 1082, 856, 788 cm^{-1}.

Crystallographic data determination: Block crystals of JUC-106 was picked for X-ray structural analysis on a Bruker SMART CCD diffractometer with a $Mo_{K\alpha}$ radiation source (λ = 0.71073 Å) at 293 K. The structure was solved and refined by full-matrix least-squares methods on F^2 values (SHELXL-97).[17] Non-hydrogen atoms were refined anisotropically. Hydrogen atoms were fixed at calculated positions and refined using a riding mode. It is unable to locate the hydrogen atoms of the water molecule. The large volume fractions of disordered solvents in the lattice pores could not be modelled in terms of atomic sites. SQUEEZE routine in PLATON was used to remove the contribution of the electron density by the remaining guest molecules.

CCDC-804509, 896050, 955370 contain the supplementary crystallographic data for this paper. These data can be obtained free of charge from The Cambridge Crystallographic Data Centre via www.ccdc.cam.ac.uk/data_request/cif.

Acknowledgements

We are grateful for the financial support of National Basic Research Program of China (973 Program, 2012CB821700), Major International (Regional) Joint Research Project of NSFC (21120102034), and National Natural Science Foundationof China (20831002; 20502024; 21374113) and Australian Research Council Future Fellowship (FT100101059).

Keywords: adsorption · computer chemistry · metal–organic frameworks · light hydrocarbons · separation

[1] a) Y. B. He, Z. J. Zhang, S. C. Xiang, H. Wu, F. R. Fronczek, W. Zhou, R. Krishna, M. O'Keeffe, B. L. Chen, *Chem. Eur. J.* **2012**, *18*, 1901 – 1904; b) S. Horike, Y. Inubushi, T. Hori, T. Fukushima, S. Kitagawa, *Chem. Sci.* **2012**, *3*, 116 – 120; c) Y. B. He, R. Krishna, B. L. Chen, *Energy Environ. Sci.* **2012**, *5*, 9107 – 9120; d) H. Xu, J. F. Cai, S. C. Xiang, Z. J. Zhang, C. D. Wu, X. T. Rao, Y. J. Cui, Y. Yang, R. Krishna, B. L. Chen, G. D. Qian, *J. Mater. Chem. A* **2013**, *1*, 9916 – 9921; e) H. Wu, Q. Gong, D. H. Olson, J. Li, *Chem. Rev.* **2012**, *112*, 836 – 868; f) Z. R. Herm, E. D. Bloch, J. R. Long, *Chem. Mater.* **2014**, *26*, 323 – 338; g) C. Y. Lee, Y. S. Bae, N. C. Jeong, O. K. Farha, A. A. Sarjeant, C. L. Stern, P. Nickias, R. Q. Snurr, J. T. Hupp, S. T. Nguyen, *J. Am. Chem. Soc.* **2011**, *133*, 5228 – 5231; h) Y. S. Bae, C. Y. Lee, K. C. Kim, O. K. Farha, P. Nickias, J. T. Hupp, S. T. Nguyen, R. Q. Snurr, *Angew. Chem.* **2012**, *124*, 1893 – 1896; *Angew. Chem. Int. Ed.* **2012**, *51*, 1857 – 1860; i) K. H. Li, D. H. Olson, J. Seidel, T. J. Emge, H. W. Gong, H. P. Zeng, J. Li, *J. Am. Chem. Soc.* **2009**, *131*, 10368; j) J. W. Yoon, Y. K. Seo, Y. K. Hwang, J. S. Chang, H. Leclerc, S. Wuttke, P. Bazin, A. Vimont, M. Daturi, E. Bloch, P. L. Llewellyn, C. Serre, P. Horcajada, J. M. Greneche, A. E. Rodrigues, G. Ferey, *Angew. Chem.* **2010**, *122*, 6085 – 6088; *Angew. Chem. Int. Ed.* **2010**, *49*, 5949 – 5952; k) U. Böhme, B. Barth, C. Paula, A. Kuhnt, W. Schwieger, A. Mundstock, J. Caro, M. Hartmann, *Langmuir* **2013**, *29*, 8592 – 8600; l) Z. B. Bao, S. Alnemrat, L. Yu, I. Vasiliev, Q. L. Ren, X. Y. Lu, S. G. Deng, *Langmuir* **2011**, *27*, 13554 – 13562.

[2] a) J. Sculley, D. Q. Yuan, H. C. Zhou, *Energy Environ. Sci.* **2011**, *4*, 2721 – 2735; b) L. J. Murray, M. Dinca, J. R. Long, *Chem. Soc. Rev.* **2009**, *38*, 1294 – 1314; c) Y. B. He, W. Zhou, T. Yildirim, B. L. Chen, *Energy Environ. Sci.* **2013**, *6*, 2735 – 2744.

[3] J. R. Li, R. J. Kuppler, H. C. Zhou, *Chem. Soc. Rev.* **2009**, *38*, 1477 – 1504.

[4] M. D. Allendorf, C. A. Bauer, R. K. Bhakta, R. J. T. Houk, *Chem. Soc. Rev.* **2009**, *38*, 1330 – 1352.

[5] L. Q. Ma, C. Abney, W. B. Lin, *Chem. Soc. Rev.* **2009**, *38*, 1248 – 1256.

[6] a) C. A. Kent, B. P. Mehl, L. Ma, J. M. Papanikolas, T. J. Meyer, W. Lin, *J. Am. Chem. Soc.* **2010**, *132*, 12767 – 12769; b) C. Y. Lee, O. K. Farha, B. J. Hong, A. A. Sarjeant, S. T. Nguyen, J. T. Hupp, *J. Am. Chem. Soc.* **2011**, *133*, 15858 – 15861.

[7] a) S. J. Geier, J. A. Mason, E. D. Bloch, W. L. Queen, M. R. Hudson, C. M. Brown, J. R. Long, *Chem. Sci.* **2013**, *4*, 2054 – 2061; b) E. D. Bloch, W. L. Queen, R. Krishna, J. M. Zadrozny, C. M. Brown, J. R. Long, *Science* **2012**, *335*, 1606 – 1610.

[8] J. T. Jia, F. X. Sun, T. Borjigin, H. Ren, T. T. Zhang, Z. Bian, L. X. Gao, G. S. Zhu, *Chem. Commun.* **2012**, *48*, 6010 – 6012.

[9] J. T. Jia, F. X. Sun, Q. R. Fang, X. Q. Liang, K. Cai, Z. Bian, H. J. Zhao, L. X. Gao, G. S. Zhu, *Chem. Commun.* **2011**, *47*, 9167 – 9169.

[10] J. Jia, F. Sun, H. Ma, L. Wang, K. Cai, Z. Bian, L. Gao, G. Zhu, *J. Mater. Chem. A* **2013**, *1*, 10112.

[11] a) J. Seo, H. Chun, *Eur. J. Inorg. Chem.* **2009**, 4946 – 4949; b) J. S. Qin, D. Y. Du, W. L. Li, J. P. Zhang, S. L. Li, Z. M. Su, X. L. Wang, Q. Xu, K. Z. Shao, Y. Q. Lan, *Chem. Sci.* **2012**, *3*, 2114 – 2118; c) S. L. Li, Y. Q. Lan, H. Sakurai, Q. Xu, *Chem. Eur. J.* **2012**, *18*, 16302 – 16309.

[12] T. Düren, L. Sarkisov, O. M. Yaghi, R. Q. Snurr, *Langmuir* **2004**, *20*, 2683 – 2689.

[13] a) H. H. Wu, K. X. Yao, Y. H. Zhu, B. Y. Li, Z. Shi, R. Krishna, J. Li, *J. Phys. Chem. C* **2012**, *116*, 16609 – 16618; b) Y. B. He, S. C. Xiang, Z. J. Zhang, S. S. Xiong, C. D. Wu, W. Zhou, T. Yildirim, R. Krishna, B. L. Chen, *J. Mater. Chem. A* **2013**, *1*, 2543 – 2551.

[14] a) S. C. Xiang, Y. He, Z. Zhang, H. Wu, W. Zhou, R. Krishna, B. Chen, *Nat. Commun.* **2012**, *3*, 954; b) R. Krishna, J. R. Long, *J. Phys. Chem. C* **2011**, *115*, 12941 – 12950; c) R. Krishna, J. M. van Baten, *Sep. Purif. Technol.* **2012**, *87*, 120 – 126; d) R. Krishna, R. Baur, *Sep. Purif. Technol.* **2003**, *33*, 213 – 254.

[15] a) Z. R. Herm, B. M. Wiers, J. M. Van Baten, M. R. Hudson, P. Zajdel, C. M. Brown, N. Maschiocchi, R. Krishna, J. R. Long, *Science* **2013**, *340*, 960 – 964; b) J. Yang, R. Krishna, J. Li, J. Li, *Microporous Mesoporous Mater.* **2014**, *184C*, 21 – 27.

[16] A. L. Myers, J. M. Prausnitz, *AIChE J.* **1965**, *11*, 121 – 130.

[17] A. L. Spek, *J. Appl. Crystallogr.* **2003**, *36*, 7 – 13.

Received: December 19, 2013
Revised: February 2, 2014
Published online on June 11, 2014

CHEMISTRY
A European Journal

Supporting Information

The Adsorption and Simulated Separation of Light Hydrocarbons in Isoreticular Metal–Organic Frameworks Based on Dendritic Ligands with Different Aliphatic Side Chains

Jiangtao Jia,[a] Lei Wang,[a] Fuxing Sun,[a] Xiaofei Jing,[a] Zheng Bian,*[b] Lianxun Gao,[b] Rajamani Krishna,[d] and Guangshan Zhu*[a, c]

chem_201304962_sm_miscellaneous_information.pdf

1. Crystal data.

Table S1 Crystal data and structure refinement for JUC-100, JUC-103 and JUC-106 single crystals.

Complex	JUC-100	JUC-103	JUC-106
Empirical formula	C_{66} H_{36} O_{13} Zn_4	C_{69} H_{42} O_{14} Zn_4	C_{72} H_{48} O_{13} Zn_4
Formula weight	1298.51	1356.51	1382.58
Temperature (K)	296(2)	296(2)	296(2)
Crystal system, Space group	Trigonal, R-3c	Trigonal, R-3c	Trigonal, R-3c
Unit cell dimensions	$a = b$ = 20.4586(8)Å c = 80.370(3)Å $\alpha = \beta$ = 90° γ = 120°	$a = b$ =19.8906(7)Å c = 83.351(6)Å $\alpha = \beta$= 90° γ = 120°	$a = b$ = 19.887(3)Å c = 83.536(17)Å $\alpha = \beta$= 90° γ = 120°
Volume (Å^3)	29132(2)	28559(2)	28613(8)
Z, Calculated density (g/cm^3)	12, 0.888	12, 0.946	12, 0.963
Absorption coefficient (mm^{-1})	1.015	1.038	1.037
F(000)	7872	8256	8448
Crystal size (mm)	0.60 x 0.55 x 0.50	0.40 x 0.30 x 0.30	0.30 x 0.30 x 0.30
θ range for data collection (°)	1.26 to 26.08	1.28 to 28.27	1.28 to 28.41
Limiting indices	-25≤h≤25 -24≤k≤25 -99≤l≤52	-21≤h≤26 -25≤k≤25 -107≤l≤110	-25≤h≤25 -25≤k≤26 -111≤l≤52
Reflections collected / unique	51924 / 6430 R_{int}= 0.0490	57010 / 7856 R_{int}=0.0452	58003 / 7992 R_{int}= 0.0533
Completeness to θ	26.08, 100.0 %	28.27, 99.6 %	26.50, 100.0 %
Absorption correction	Semi-empirical from equivalents	Semi-empirical from equivalents	Semi-empirical from equivalents
Max. and min. transmission	0.602 and 0.549	0.7458 and 0.6815	0.7462 and 0.7462
Refinement method	Full-matrix least-squares on F^2	Full-matrix least-squares on F^2	Full-matrix least-squares on F^2
Data / restraints / parameters	6430 / 18 / 250	7856 / 6 / 262	7992 / 0 / 268
Goodness-of-fit on F^2	1.061	1.055	0.974
Final R indices [I > 2sigma(I)]	R_1 =0.0743, wR_2 = 0.2258	R_1 = 0.0773 wR_2 = 0.2536	R_1 = 0.0663 wR_2 = 0.1976
R indices (all data)	R_1 =0.0877 wR_2 = 0.2375	R_1 =0.1015 wR_2 = 0.2763	R_1 = 0.0905 wR_2 = 0.2155
Largest diff. peak and hole (e.Å^{-3})	1.731 and -2.137	1.461 and -3.265	1.075 and -2.590
CCDC	804509	896050	955370

2. Fitting of pure component isotherms for JUC-100, JUC-103, and JUC-106.

The experimentally measured excess loadings of CH_4, C_2H_4, C_2H_6, and C_3H_8, obtained at temperatures at 298 K for JUC-100, JUC-103, and JUC-106 were first converted to absolute loadings before data fitting. For this purpose the pore volume used were: JUC-100: 0.954 cm^3/g; JUC-103: 0.576 cm^3/g; JUC-106: 0.427 cm^3/g. The procedure for converting excess loadings to absolute loadings is described in detail in the Supporting Information accompanying the paper by Wu et al.[1]

The isotherm data for both materials were fitted with the single-site Langmuir model

$$q = q_{sat}\frac{bp}{1+bp} \quad (1)$$

The Langmuir fit parameters are listed in Table S2.

Figure S1 provides a comparison of the absolute component loadings of CH_4, C_2H_4, C_2H_6, and C_3H_8, obtained at temperatures at 298 K for JUC-100, JUC-103, and JUC-106 with the single-site Langmuir fits using the parameter sets presented in Table S2. The single-site Langmuir model is of excellent accuracy for all guest-host combinations. A close examination of the data indicates that the adsorption loadings decrease with decrease pore volumes as we proceed from JUC-100, to JUC-103 to JUC-106. In other words, decreasing pore volume results in a decreased adsorption uptake capacity. This has implications for the transient breakthroughs in fixed bed adsorbers.

3. IAST calculations of adsorption selectivity.

The selectivity of preferential adsorption of component 1 over component 2 in a mixture containing 1 and 2, perhaps in the presence of other components too, can be formally defined as

$$S_{ads} = \frac{q_1/q_2}{p_1/p_2} \quad (2)$$

In equation (2), q_1 and q_2 are the *absolute* component loadings of the adsorbed phase in the mixture. In all the calculations to be presented below, the calculations of S_{ads} are based on the use of the Ideal Adsorbed Solution Theory (IAST) of Myers and Prausnitz.[2]

Figure S1 presents the IAST calculations of C_3H_8/CH_4, C_2H_6/CH_4, and C_2H_6/C_2H_4 selectivities for equimolar quaternary $CH_4/C_2H_4/C_2H_6/C_3H_8$ gas mixture maintained at isothermal conditions at 298 K.

4. Packed bed adsorber breakthrough simulations.

The separation of light hydrocarbon mixtures is normally carried out within industry using fixed bed adsorbers. The performance of fixed bed adsorbers is dictated by both selectivity and capacity considerations. In order to demonstrate the potential of JUC-100, JUC-103, and JUC-106 for separation of light hydrocarbons we carried out simulations of transient breakthroughs of equimolar 4-component quaternary $CH_4/C_2H_4/C_2H_6/C_3H_8$ gas mixture maintained at isothermal conditions at 298 K and 100 kPa, with partial pressures for each component of 25 kPa. The methodology used for the breakthrough simulations are the same as described in earlier works.[1, 3-8] Experimental validation of the breakthrough simulation methodology is available in the published literature.[1, 4, 9-11]

Figure S2 shows a schematic of a packed bed adsorber packed with JUC-100, JUC-103, or JUC-106. The following parameter values were used: length of packed bed, L = 0.1 m; fractional voidage of packed bed, ε = 0.4; superficial gas velocity at inlet of adsorber, u = 0.04 m/s, framework density of JUC-100, ρ = 888 kg/m^3; JUC-103, ρ =933kg/m^3; JUC-106, ρ =963kg/m^3.

Table S2 Langmuir fit parameters for CH_4, C_2H_4, C_2H_6, C_3H_6, and C_3H_8 in JUC-100, JUC-103, and JUC-106 at 298 K.

	JUC-100		JUC-103		JUC-106	
	q_{sat}	b	q_{sat}	b	q_{sat}	b
	mol kg^{-1}	Pa^{-1}	mol kg^{-1}	Pa^{-1}	mol kg^{-1}	Pa^{-1}
CH_4	20	2.68×10^{-7}	20	2.91×10^{-7}	15	2.72×10^{-7}
C_2H_4	9.5	4.82×10^{-6}	9.5	4.76×10^{-6}	7	4.83×10^{-6}
C_2H_6	8.8	9.44×10^{-6}	8	9.14×10^{-6}	7.5	9.01×10^{-6}
C_3H_8	6.7	1.2×10^{-4}	6	1.13×10^{-4}	5.6	9.78×10^{-5}

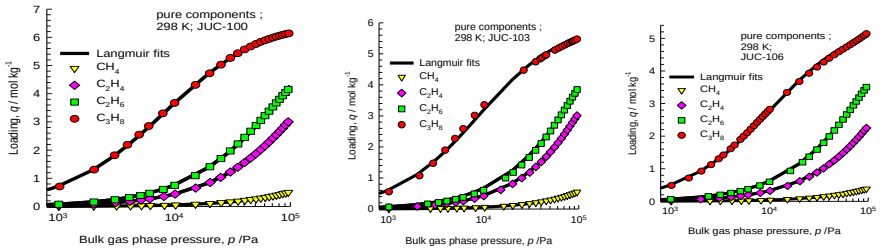

Figure S1 Comparison of the absolute component loadings of CH_4, C_2H_4, C_2H_6, and C_3H_8, obtained at temperatures at 298 K for (left) JUC-100, (middle) JUC-103, and (right) JUC-106 with the single-site Langmuir fits using the parameter sets presented in Table S2

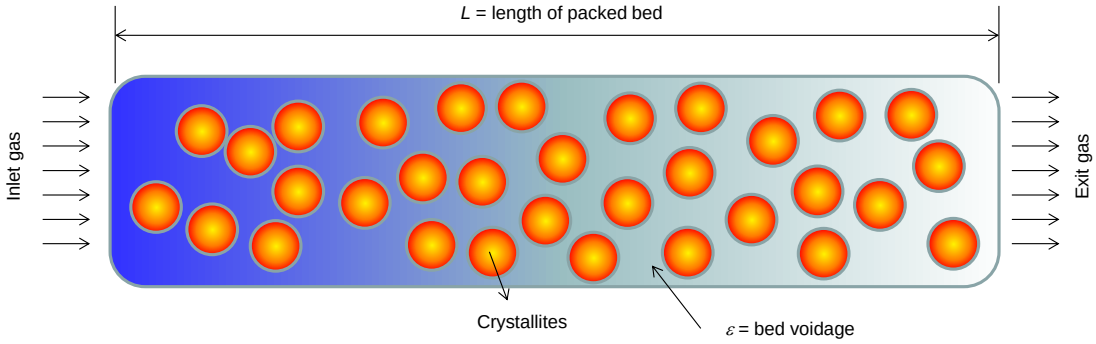

Figure S2 Schematic of a packed bed adsorber.

5. Notation.

b	Langmuir constant, Pa^{-1}
c_i	molar concentrations of species i in gas mixture, mol m^{-3}
c_{i0}	molar concentrations of species i in gas mixture at inlet to adsorber, mol m^{-3}
L	length of packed bed adsorber, m
p_i	partial pressure of species i in mixture, Pa
p_t	total system pressure, Pa
q_i	component molar loading of species i, mol kg^{-1}
q_{sat}	saturation loading, mol kg^{-1}
S_{ads}	adsorption selectivity, dimensionless

t	time, s
T	absolutetemperature, K
u	superficial gas velocity in packed bed, m s^{-1}
z	distance along the adsorber, m

Greek letters.

ε	voidage of packed bed, dimensionless
ρ	framework density, kg m^{-3}
τ	time, dimensionless

6. References.

(1) Wu, H.; Yao, K.; Zhu, Y.; Li, B.; Shi, Z.; Krishna, R.; Li, J. Cu-TDPAT, an *rht*-type Dual-Functional Metal–Organic Framework Offering Significant Potential for Use in H_2 and Natural Gas Purification Processes Operating at High Pressures, *J. Phys. Chem. C*, **2012**, *116*,16609-16618.

(2) Myers, A. L.; Prausnitz, J. M. Thermodynamics of mixed gas adsorption, *A. I. Ch. E .J.*, **1965**, *11*,121-130.

(3) Xiang, S. C.; He, Y.; Zhang, Z.; Wu, H.; Zhou, W.; Krishna, R.; Chen, B. Microporous Metal-Organic Framework with Potential for Carbon Dioxide Capture at Ambient Conditions, *Nat. Commun.*, **2012**, *3*,954.

(4) He, Y.; Krishna, R.; Chen, B. Metal-Organic Frameworks with Potential for Energy-Efficient Adsorptive Separation of Light Hydrocarbons, *Energy Environ. Sci.*, **2012**, *5*,9107-9120.

(5) He, Y.; Xiang, S.; Zhang, Z.; Xiong, S.; Wu, C.; Zhou, W.; Yildirim, T.; Krishna, R.; Chen, B. A microporous metal-organic framework assembled from an aromatic tetracarboxylate for H_2 purification, *J. Mater. Chem. A*, **2013**, *1*,2543-2551.

(6) Krishna, R.; Long, J. R. Screening metal-organic frameworks by analysis of transient breakthrough of gas mixtures in a fixed bed adsorber, *J. Phys. Chem. C*, **2011**, *115*,12941-12950.

(7) Krishna, R.; van Baten, J. M. A comparison of the CO_2 capture characteristics of zeolites and metal-organic frameworks, *Sep. Purif. Technol.*, **2012**, *87*,120-126.

(8) Krishna, R.; Baur, R. Modelling issues in zeolite based separation processes, *Sep. Purif. Technol.*, **2003**, *33*, 213-254.

(9) Bloch, E. D.; Queen, W. L.; Krishna, R.; Zadrozny, J. M.; Brown, C. M.; Long, J. R. Hydrocarbon Separations in a Metal-Organic Framework with Open Iron(II) Coordination Sites, *Science*, **2012**, *335*,1606-1610.

(10) Herm, Z. R.; Wiers, B. M.; Van Baten, J. M.; Hudson, M. R.; Zajdel, P.; Brown, C. M.; Maschiocchi, N.; Krishna, R.; Long, J. R. Separation of Hexane Isomers in a Metal-Organic Framework with Triangular Channels, *Science*, **2013**, *340*, 960-964.

(11) Yang, J.; Krishna, R.; Li, J.; Li, J. Experiments and Simulations on Separating a CO_2/CH_4 Mixture using K-KFI at Low and High Pressures, *Microporous Mesoporous Mater.*, **2014**, *184*, 21-27.

7. Asymmetrical unit of JUC-106.

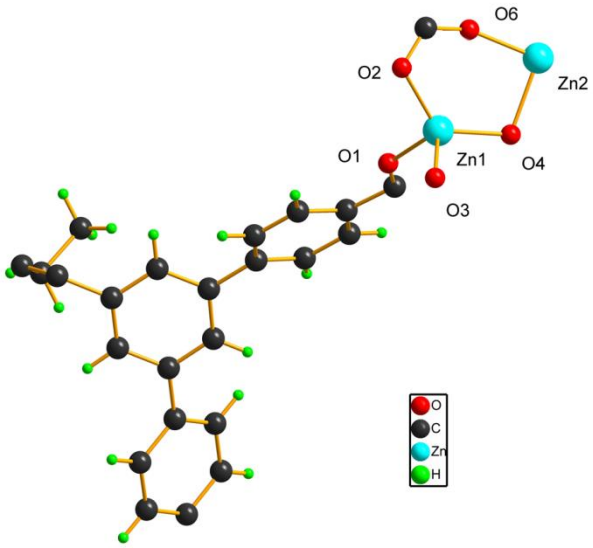

Figure S3 Asymmetrical unit of JUC-106

8. XRD patterns of JUC-106.

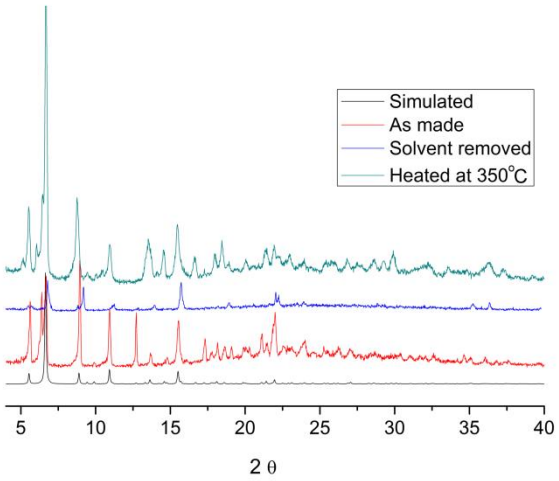

Figure S4 XRD patterns of JUC-106

9. The distances between two interpenetrated structures.

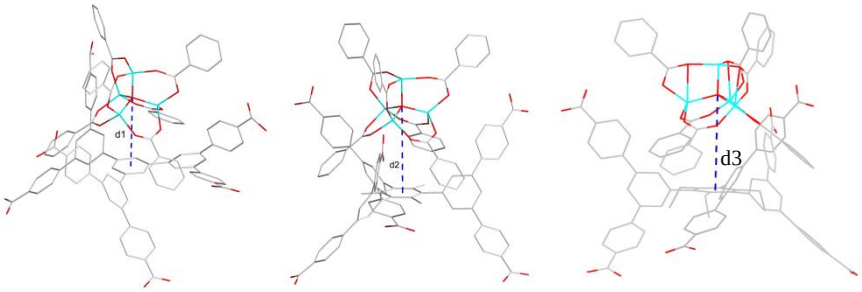

Figure S5 The distances of two interpenetrated structures in JUC-100 (left), JUC-103 (middle) and JUC-106 (right), d1 = 5.609 Å, d2 = 6.418 Å and d3 = 6.457 Å.

10. TG curve of JUC-106.

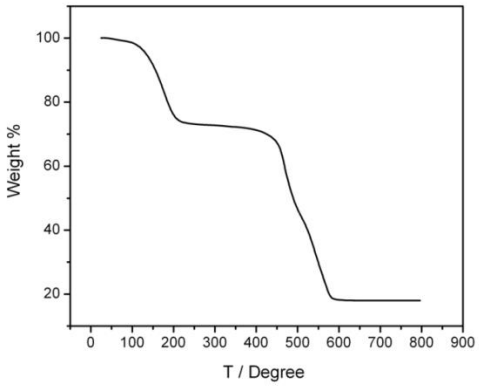

Figure S6 TG curve JUC-106.

11. Heat of absorption for gas of JUC-100, JUC-103 and JUC-106.

The heat of the adsorption is calculated by virial-type equation.

$$\ln P = \ln N + \frac{1}{T}\sum_{i=0}^{m} a_i N^i + \sum_{i=0}^{m} b_i N^i \qquad (1)$$

$$Q_{st} = -R\sum_{i=0}^{m} a_i N^i \qquad (2)$$

We used the equation to fit the adsorption data of C_3H_8 adsorption. However, the fitting error is very large. At 273 K, 0.01 atm, the uptakes of these three MOFs were larger than 40 cc/g. Because our measurement machine for adsorption cannot collect the data at lower than 0.01 atm, the uptake below 40 cc/g was not obtained. We speculated that the missing of the data below 40 cc/g could produce the fitting error. So, we did not give the adsorption heat of C_3H_8.

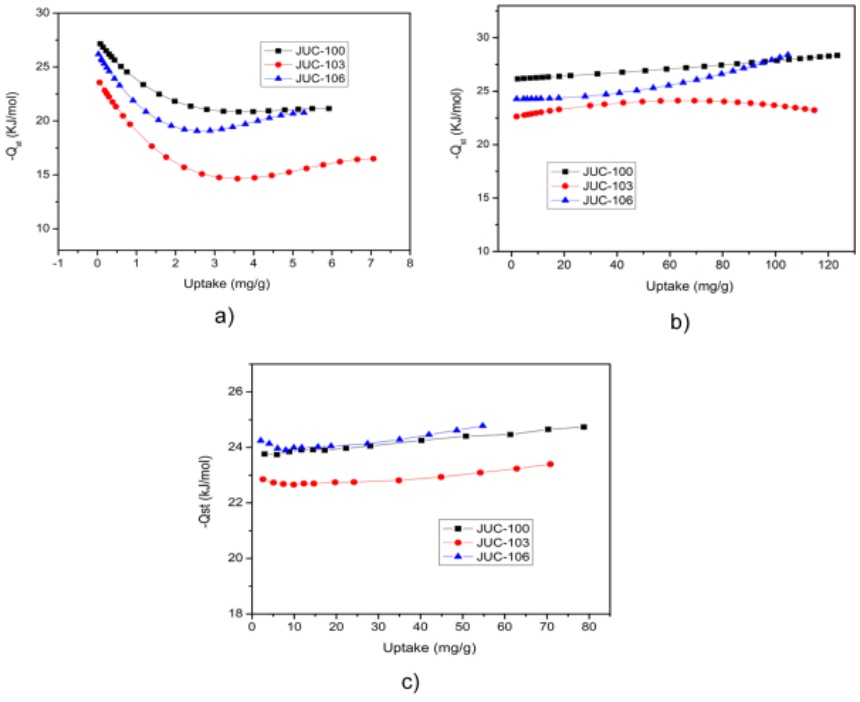

Figure S7 The heats of absorption for CH_4 (a), C_2H_6 (b) and C_2H_4 (c) of JUC-100, JUC-103 and JUC-106